Three-dimensional Analytical Models for Predicting Coating Thickness on Non-axial Symmetrical Workpieces in Electron Beam Physical Vapor Deposition

Yafeng Li[1], Zhengzhao Ji[1], Anvesh Dhulipalla[2], Jian Zhang[2], Xuehui Yang[2], Tejesh Dube[2], Bong-Gu Kim[3], Yeon-Gil Jung[3], Dan Daehyun Koo[4], Jing Zhang[2,*]

1. Tianjin Key Laboratory of Modern Mechatronics Equipment Technology, Tiangong University, Tianjin, P.R. China
2. Department of Mechanical and Energy Engineering, Indiana University - Purdue University Indianapolis, USA
3. Department of Materials Convergence and System Engineering, Changwon National University, Republic of Korea
4. Department of Engineering Technology, Indiana University - Purdue University Indianapolis, USA
*Corresponding author: jz29@iupui.edu

Abstract

In this work, three-dimensional (3D) analytical models for non-axial symmetric workpieces, including ellipsoid and cylinder, are derived to predict the coating thickness distributions in the EB-PVD process. Additionally, 3D analytical models for axial symmetric workpieces, including disk and sphere are presented, which will be used for deriving the non-axial symmetric workpiece solutions. The models are based on extending the two-dimensional (2D) models of a disk workpiece by Schiller [1] and a circular arc on a cylinder by Fuke [2]. The 3D models for disk and sphere workpieces are also presented which are used to derive the non-axial symmetric models. The results show that the 3D analytical models are consistent with the 2D models, and also in excellent agreement with our finite element (FE) model predictions and experimental data in the literature.

Keywords: Coating thickness; Ray-tracing method; Geometry analytical solution

---

This is the author's manuscript of the article published in final edited form as:

Li, Y., Ji, Z., Dhulipalla, A., Zhang, J., Yang, X., Dube, T., Kim, B.-G., Jung, Y.-G., Koo, D. D., & Zhang, J. (2022). Three-dimensional analytical models for predicting coating thickness on non-axial symmetrical workpieces in electron beam physical vapor deposition. CIRP Journal of Manufacturing Science and Technology, 38, 268–273. https://doi.org/10.1016/j.cirpj.2022.05.006

Nomenclature

Parameter	Description	Unit
d_{s0}	Maximum film thickness for α_1, α_2=0	mm
α_1, α_2	Angles of divergence in *x*-, *y*-direction, respectively	°
α	Angle of divergence from the source for symmetric workpiece	
h_v	Distance of workpiece and coating source	mm
h'	Height of any point above h_v	mm
n	Index on evaporation rate (2 ~ 6)	
θ	Inclination angle of the tangent	°
r_s	Distance from maximum point thickness	mm
t	Position coefficient for cylinder	
a, b	Major axis and minor axis of ellipsoid	mm
d_{sd_3d}	Disk local film thickness	mm
d_{sc_3d}	Cylinder local film thickness	mm
d_{ss_3d}	Sphere local film thickness	mm
d_{se_3d}	Ellipsoid local film thickness	mm

1 Introduction

Electron Beam Physical Vapor Deposition (EB-PVD) is an important coating technique that utilizes electron beams as a source to evaporate coating materials, which are then deposited on a substrate [3, 4]. In addition to extensive experimental studies (e.g., [5, 6]), several computational models have been developed to understand the coating thickness distributions. Based on the ray-tracing method, Fuke *et al.* [2] extended Schiller's flat plate model [1] and proposed an analytical model for the disk- and cylinder-shaped workpieces. However, only coating thickness along the middle cross-sections of the disk or cylinder is predicted, which renders the model essentially a two-dimensional (2D) model along the tangential direction [2]. Mao *et al.* proposed a neural network-based model to predict the thickness in a hot-dip galvanization plate [7]. Cho applied a heuristic algorithm to optimize the uniformity of coating thickness and substrate temperature [8]. Xie *et al.* studied the influence of the spraying parameters on the spray flow field and coating thickness distribution during the air spray process [9]. Pereira *et al.* developed a computational model with the shadow effect taken into consideration [10]. Pereira's model is applied to predict the coating thickness distribution in a three-pin rotatory component [10].

Although the above-mentioned effort, a three-dimensional (3D) analytical model for coating prediction is still needed. Analytical models have the advantage of being easy to use for fast calculations, which can be used as a first-order estimation. Additionally, analytical models can be used as a benchmark solution for other types of computational models. In this work, we propose the three-dimensional analytical models for coating thickness on non-axial symmetrical workpieces, including ellipsoid and cylinder. Special cases, such as disk and sphere substrates, are also presented. We demonstrate that our 3D models have good agreement with reduced 2D models and finite element (FE) models.

2 Derivations of 3D analytical solutions for coating thickness

In this section, the detailed derivations of each shape workpiece are presented. It is noted that, in real applications, the evaporation pool on the target surface has a spatical size. In this work, a point-like source is assumed in the model, which is needed for deriving the analytical solutions.

Additionally, the coating thickness of the same shape workpiece is calculated using the finite element method, as presented in our recent work [11]. Our previous finite element model for coating thickness prediction [11] has the major advantage of computational efficiency, which is faster than the traditional ray-tracing based model by about two orders of magnitude. This is because the Gaussian distribution heating source used in the finite element has the same profile as the cosine relation used in the ray-tracing method. Firstly, the model simulates the temperature profile of a metal substrate heated by a heating source with a Gaussian distribution. The model is successfully demonstrated by three validation cases, including a stationary disk, a stationary cylinder, and a rotary three-pin component [11]. In this work, we apply our finite element model to simulate the coating thickness in the workpieces presented in this study, in order to compare with the derived analytical solutions.

2.1 Disk workpiece

In order to derive 3D models, first Schiller's 2D disk model [1] is revised for 3D space. Fuke's 2D disk coating thickness is [2]:

$$d_{sd_3d}/d_{s0} =\cdot \frac{1}{(1+\tan^2\alpha)^{\frac{n+3}{2}}} \tag{1}$$

Given the suggested values for n are 2~6 [2], the power term $\frac{n+3}{2}$ in Equation 1 can be reasonably to assume to be n without losing much accuracy in the angle range interested, and the coating thickness for a disk workpiece becomes:

$$d_{sd_3d}/d_{s0} =\cdot \frac{1}{(1+\tan^2\alpha)^{n}} \tag{2}$$

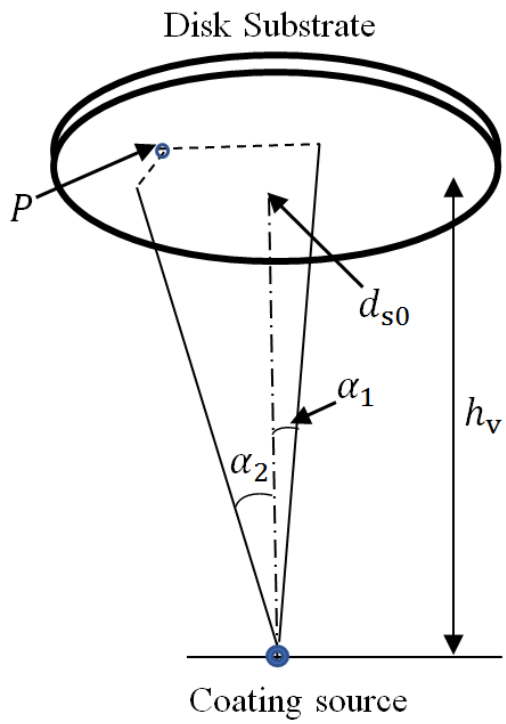

Figure 1: Disk workpiece coating process

For 3D case as shown in Figure 1, the distance between the maximum film thickness center point and any coating point, r_{sd}, is:

$$r_{sd} = h_v \cdot (\tan^2\alpha_1 + \tan^2\alpha_2)^{\frac{1}{2}} \tag{3}$$

Therefore, the 3D disk coating thickness is:

$$d_{sd_3d}/d_{s0} =\cdot \frac{1}{(1+\tan^2\alpha_1+\tan^2\alpha_2)^n} \tag{4}$$

2.2 Cylinder workpiece

Fuke's 2D solution for a cylinder workpiece is shown in Figure 2 [2]:

$$d_{sc}/d_{s0} = \left[\frac{h_v^2\cdot\cos^2\alpha}{(h_v+h')^2}\right] \cdot \cos(\alpha + \theta) \cdot \cos^{\mathrm{n}}\alpha \tag{5}$$

In this work, we extend Fuke's 2D cylinder solution $f(d_s, \alpha)$ in Equation 5 to a 3D solution $f(d_s, \alpha_1, \alpha_2)$, as shown in Figure 2. The distance between the maximum film thickness center point and any coating point on the cylinder surface is an arc, and it can be expressed as:

$$r_{sc} = \sqrt{(h_v \cdot \tan\alpha_1)^2 + \left((h_v + h') \cdot \tan\alpha_2\right)^2} \tag{6}$$

The normalized arc distance, *t*, is:

$$t = \sqrt{(h_v \cdot \tan\alpha_1)^2 + \left((h_v + h') \cdot \tan\alpha_2\right)^2} / h_v \tag{7}$$

Combining Equations 4 and 6, the coating thickness for the 3D cylinder workpiece d_{sc_3d} is derived as:

$$d_{sc_3d}/d_{s0} = (1 - t) \cdot d_1 \cdot d_2 \tag{8}$$

where $d_1$and d_2 are expressed as follows:

$$d_1 = \frac{1}{(1+\tan^2\alpha_1)^n} \tag{9}$$

$$d_2 = \left[\frac{h_v^2 \cdot \cos^2\alpha_2}{(h_v+h')^2}\right] \cdot \cos(\alpha_2 + \theta) \cdot \cos^{\mathrm{n}}\alpha_2 \tag{10}$$

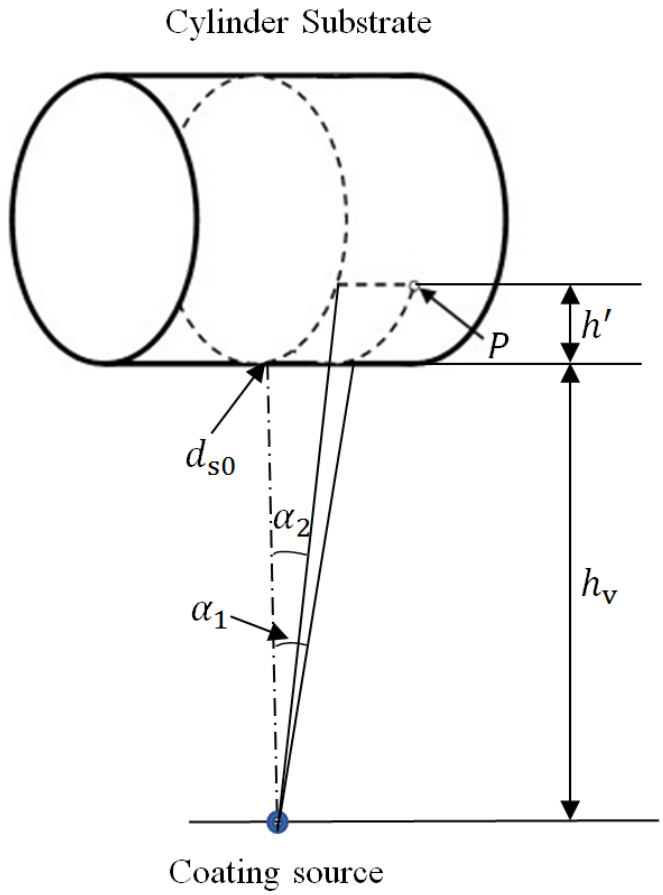

Figure 2: Cylinder workpiece coating process

2.3 Sphere workpiece

The solution of the 3D sphere workpiece thickness d_{ss_3d} can be derived by combining the 3D disk (Equation 4) and 3D cylinder (Equation 8) solutions and it becomes:

$$d_{ss_3d}/d_{s0} = \frac{h_v^2}{(h_v+h')^2} \cdot \frac{\cos^2\alpha_1 \cdot \cos^2\alpha_2}{(1+\tan^2\alpha_1+\tan^2\alpha_2)^n} \tag{11}$$

where $\frac{h_v^2}{(h_v+h')^2}$ is the position coefficient to the sphere surface; $(\cos^2\alpha_1 + \cos^2\alpha_2)$ is for calculating the thickness along the tangential direction in the 3D cylinder solution (Equation 8); and $(1 + \tan^2\alpha_1 + \tan^2\alpha_2)^n$ is the symmetry character part from the 3D disk solution (Equation 4).

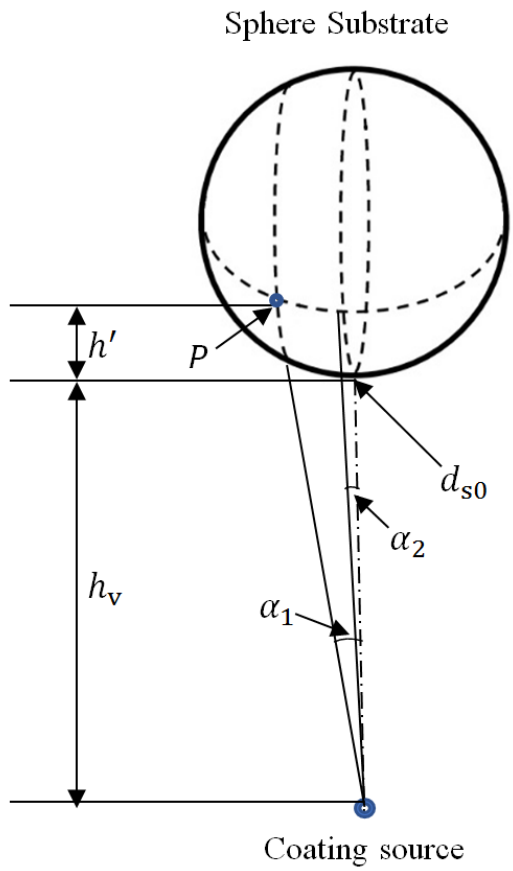

Figure 3: Sphere workpiece coating process

2.4 Ellipsoid workpiece

The ellipsoid substrate has long and short axes, expressed as a and b, respectively. The coating thickness on an ellipsoid workpiece is symmetric along the axes. The 3D ellipsoid local film thickness d_{se_3d} is determined by extending the 3D sphere solution and it becomes:

$$d_{se_3d}/d_{s0} =\cdot \frac{h_v^2}{(h_v+h')^2} \cdot \frac{ab\cdot\cos^2\alpha_1\cdot\cos^2\alpha_2}{(1+a^2\cdot\tan^2\alpha_1+b^2\cdot\tan^2\alpha_2)^n} \tag{12}$$

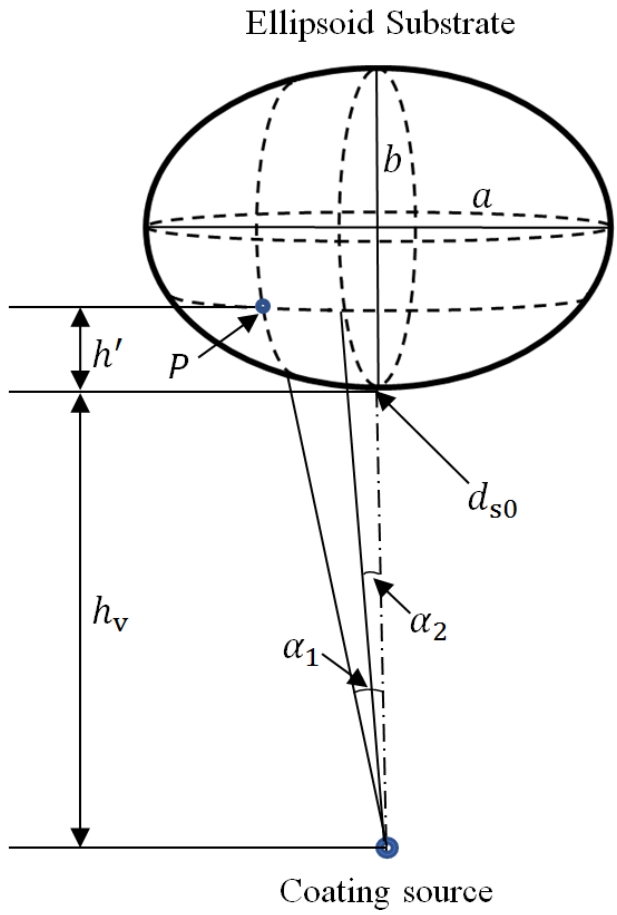

Figure 4: Ellipsoid workpiece coating process

3 Results and discussion

To evaluate the derived analytical solutions, we compare the coating thickness between the derived analytical model in this work, the finite element model presented in our recent paper [11], and experimental data in the literature.

3.1 Disk workpiece

The 3D normalized coating thickness prediction of the disk workpiece using the derived analytical model (Equation 4) is shown in Figure 5. As expected, the thickness distribution shows is axially symmetric, with a Gaussian distribution characteristic.

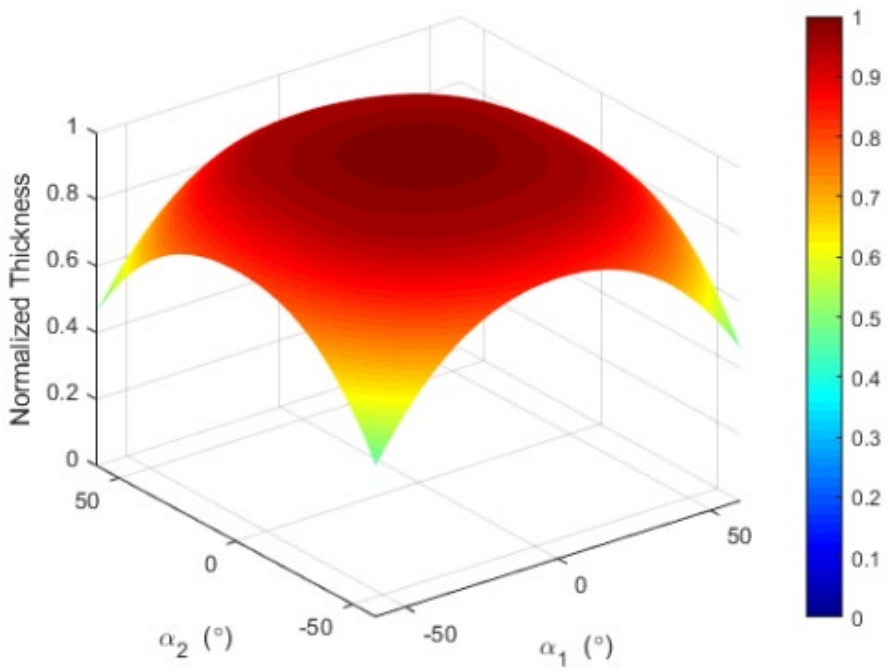

Figure 5: Predicted coating thickness distribution using the 3D analytical model (Equation 4) for a disk workpiece.

To compare with other data in the literature, the thickness along the disk diameter is plotted in Figure 6. The results from the FE model [11], Fuke's 2D analytical model [2], and Fuke's experimental data [2] are also included. Our 3D analytical model agrees well with other models and experimental data, suggesting the validity of our 3D analytical model.

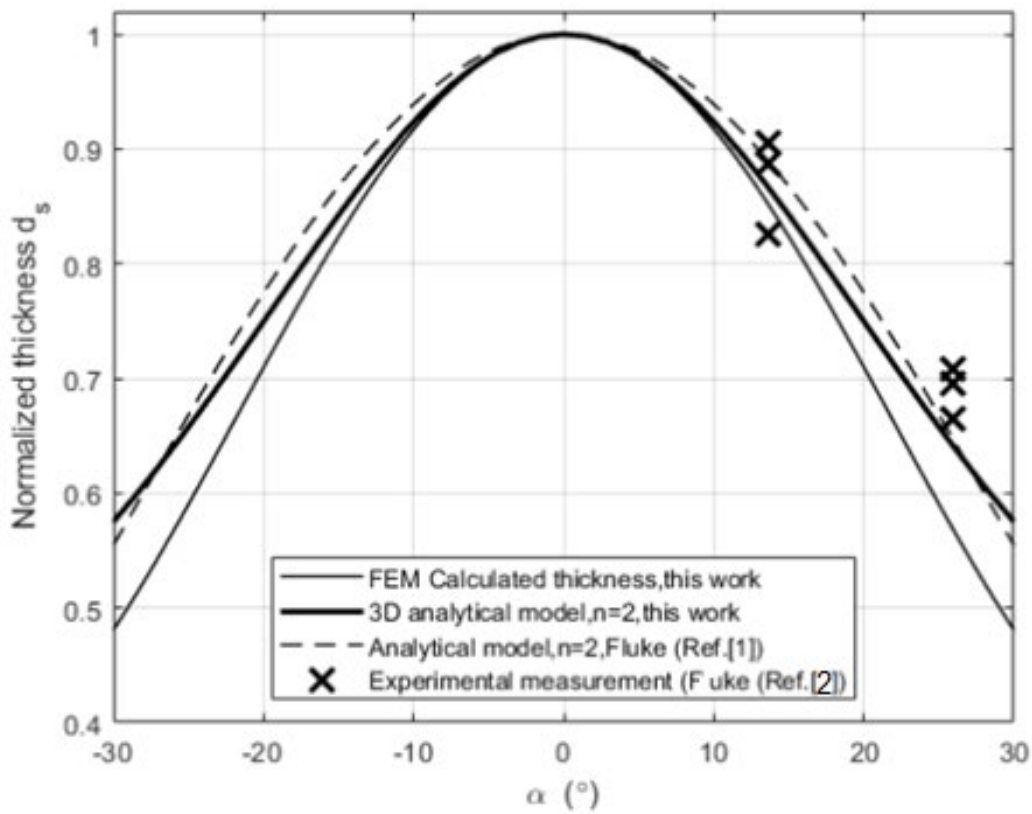

Figure 6: Normalized thickness distribution along the diameter of the disk, including 3D FE model, 3D analytical model in this study, 2D analytical model [2], and experimental data [2].

3.2 Cylinder workpiece

As shown in Figure 7, the thickness distributions along the cylinder axial direction are different from the tangential direction. The tangential direction results are plotted in Figure 8. The axial direction, which is not available in the 2D model [2], shows a more uniform distribution on the edge, suggesting the necessity of the non-axial symmetric model.

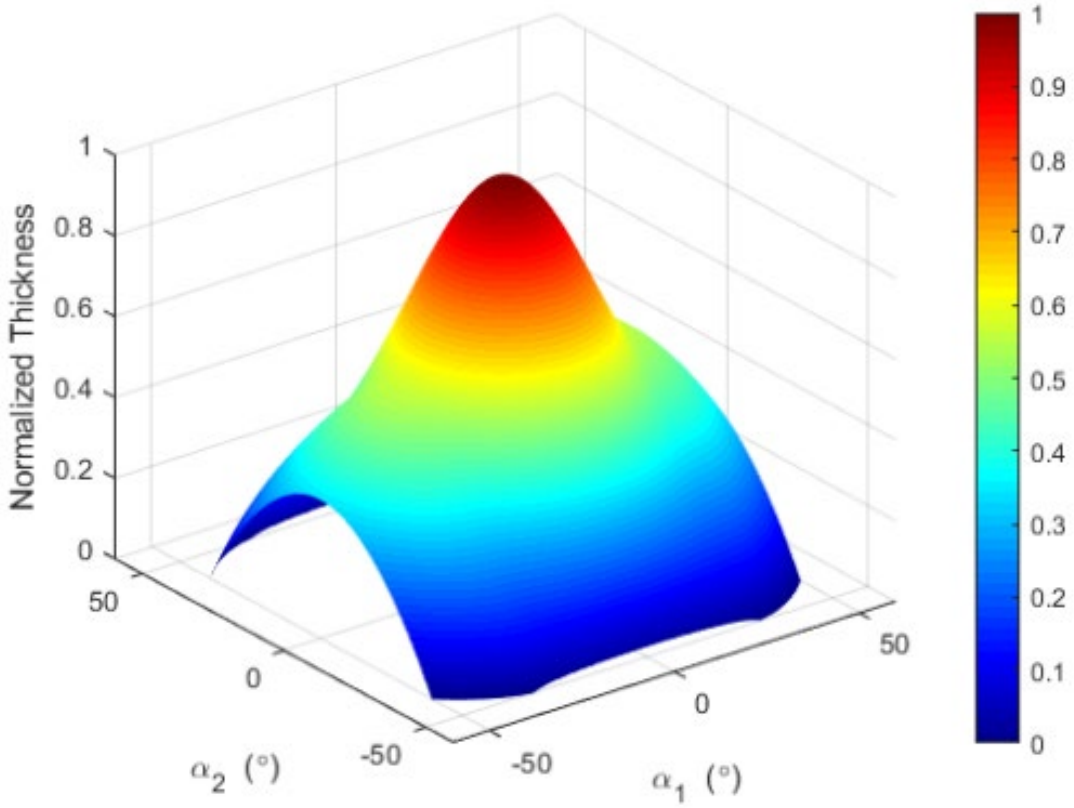

Figure 7: Predicted coating thickness distribution using the 3D analytical model (Equation 8) for a 3D cylinder workpiece.

The tangential direction results in Figure 8 show that the 3D analytical model has an excellent agreement with the FE model and Fuke's 2D axial symmetrical model [2]. Therefore the 3D analytical model can be used with confidence for predicting coating thickness in a cylinder workpiece.

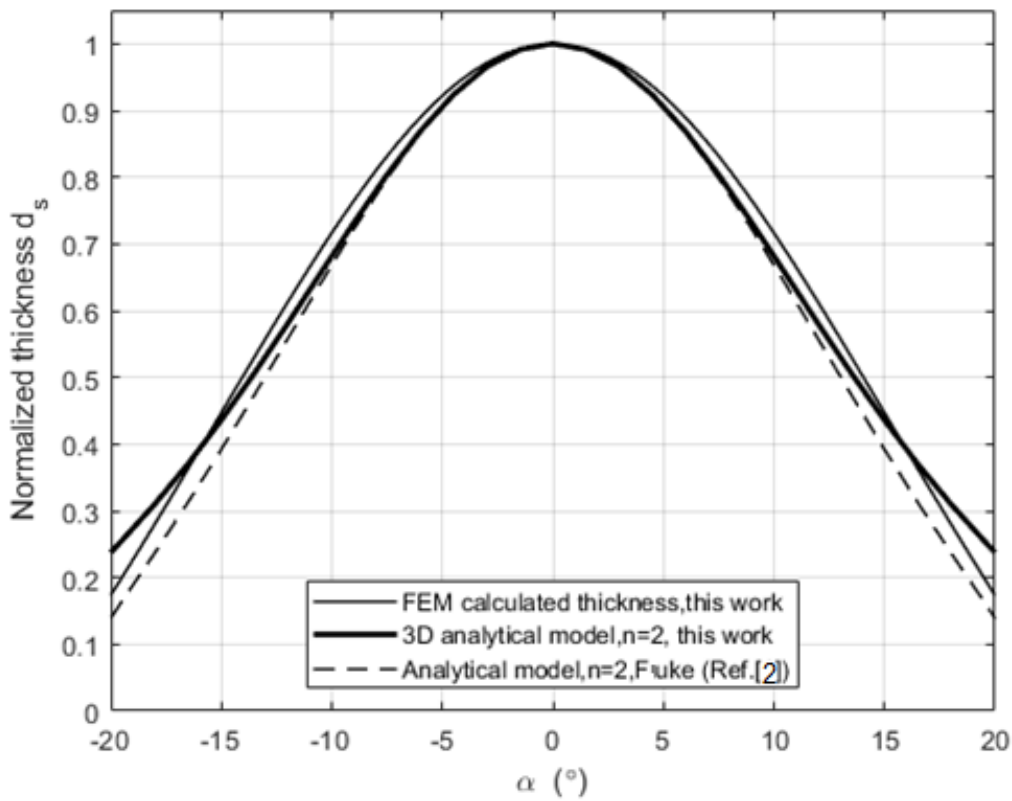

Figure 8: Normalized thickness distribution along the tangential direction of the cylinder, including the 3D analytical model in this study, the 3D FE model[11], and the 2D analytical model [2].

3.3 Sphere workpiece

The thickness distribution using the sphere model (Equation 11) is shown in Figure 9. Similar to the disk model, it shows axial symmetry, with the center as the maximum. The cross-sectional distribution shows a quadratic characteristic that was also shown in Ref. [2].

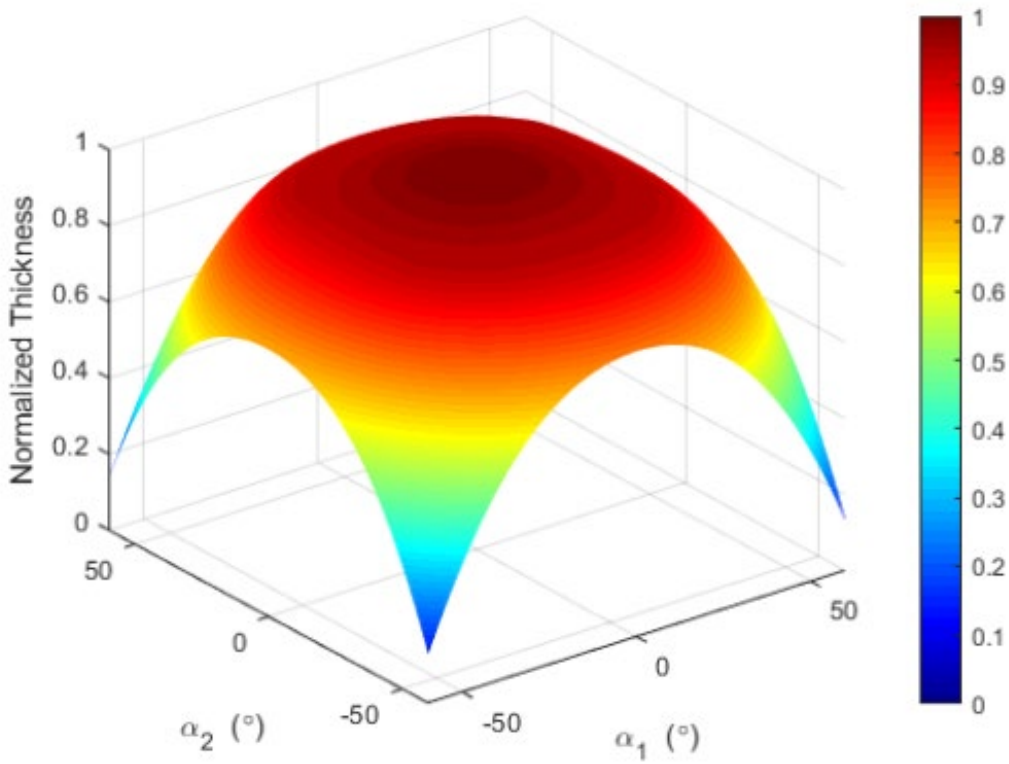

Figure 9: Predicted coating thickness distribution using the 3D analytical model (Equation 11) for a sphere workpiece.

Figure 10 shows the normalized thickness distribution on the sphere workpiece surface, using both the analytical solution and the FE model, along with the two divergence angles α_1, and α_2 It is noted that there is a small discrepancy between the two methods. This is because, in the FE model, a fitting step of the temperature distribution on the workpiece surface is required, for converting the temperature field to the coating thickness distribution [11].

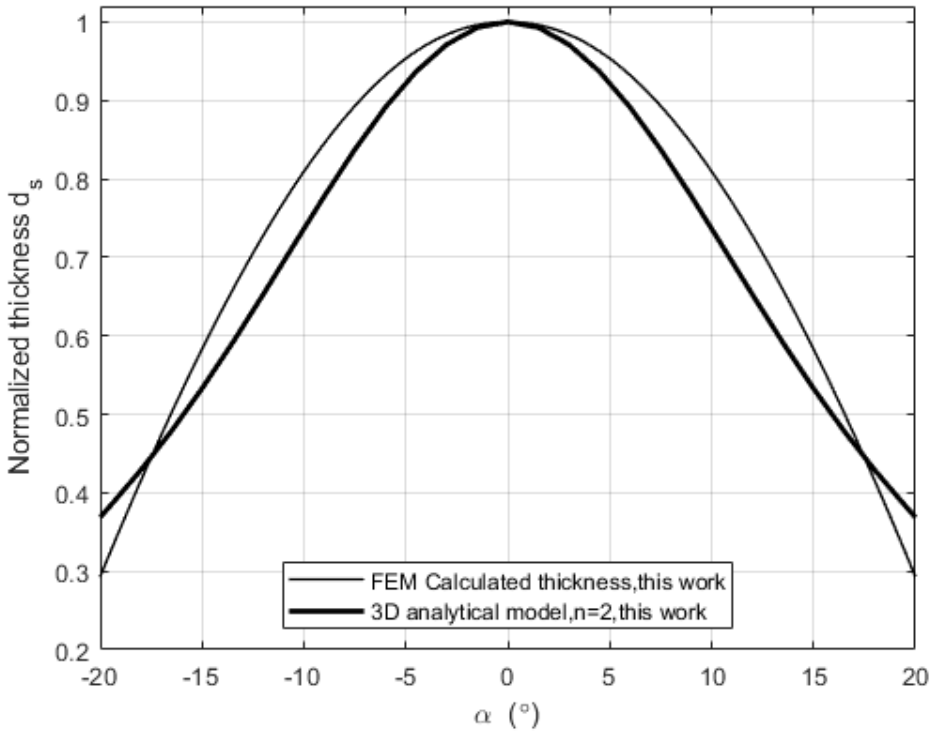

Figure 10: Normalized thickness distribution in a sphere workpiece, including 3D FEM and 3D analytical model in this study.

3.4 Ellipsoid workpiece

Using the FE model [11], the predicted thickness distributions in the sphere (a/b=1) and ellipsoids with two axis ratios (a/b = 1.5 and 2) are given in Figure 11. The sphere workpiece shows an axial symmetry, while the ellipsoid workpieces are different based on the directions.

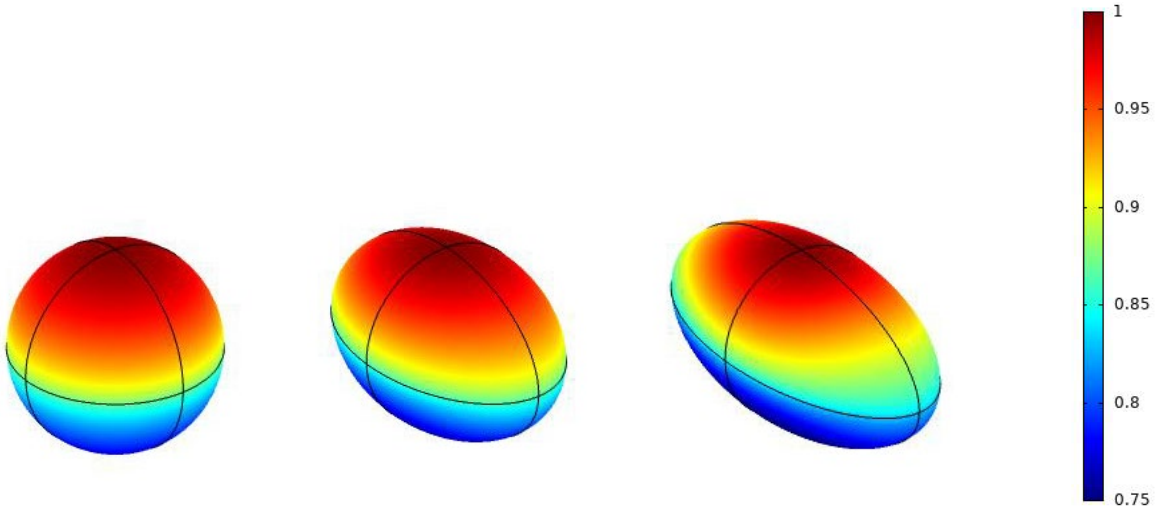

(a) (b) (c)

Figure 11: 3D FE model results of the normalized coating thickness in a 3D sphere (a/b=1), and ellipsoid (a/b=1.5 and a/b=2) workpieces.

As shown in Figure 12, the thickness distributions along the long-axis direction (case a) are different from the short-axis direction (case b). The long-axis direction has a more even thickness distribution in the α_1 angle range, indicating the need for the non-axial symmetric model.

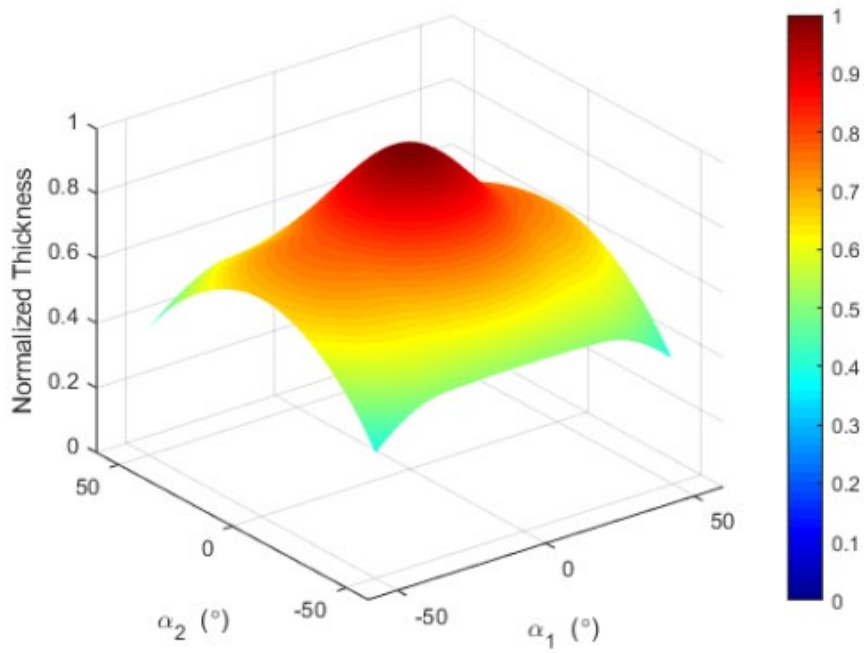

Figure 12: Predicted coating thickness distribution using the 3D analytical model (Equation 12) for an ellipsoid workpiece (a/b=2).

Due to symmetry, half of the coating thickness distributions along the ellipsoid surface are plotted, as shown in Figure 13. As the axis ratio, a/b increases from 1 to 2, the workpiece is stretched from a sphere to an elongated ellipsoid. The coating thickness is also spread along the long axis direction. Also in Figure 12, both the 3D analytical and FE models show a similar trend in the coating thickness distribution. The difference between the two models is caused by the temperature conversion procedure used in the FE model.

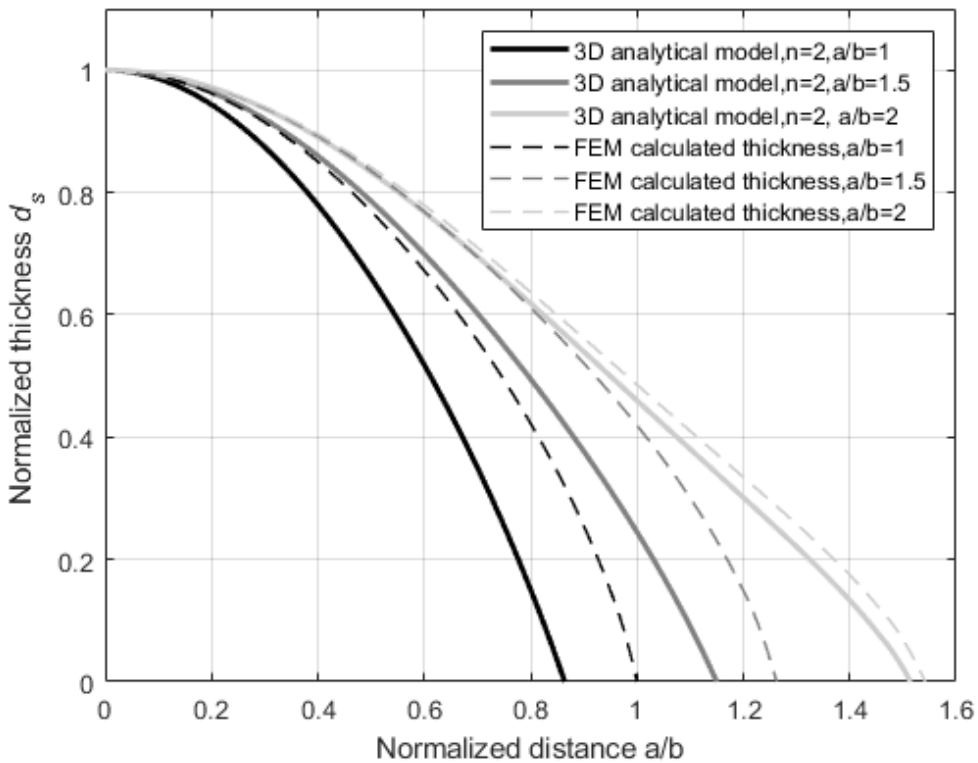

Figure 13: Normalized thickness distributions in ellipsoid workpieces in ellipsoids with different a/b ratios (a/b=1, 1.5, and 2), including the 3D FE and 3D analytical models in this study.

Conclusions

In this work, 3D analytical models for non-axial symmetric workpieces, including ellipsoid and cylinder, are derived to predict the coating thickness distributions in the EB-PVD process. Additionally, 3D analytical models for axial symmetric workpieces, including disk and sphere are presented. The major conclusions are summarized below.

1. For the disk workpiece, the derived 3D analytical model agrees well with the FE model, Fuke's 2D analytical model, and experimental data, suggesting the validity of our 3D analytical model.
2. For the cylinder workpiece, the 3D model shows that the axial direction, which is not available in Fuke's 2D model, has a more uniform distribution on the edge, suggesting the necessity of the non-axial symmetric model.

3. For the sphere workpiece, similar to the disk model, there is an axial symmetry. The cross-sectional distribution in the 3D model shows a quadratic characteristic, the same as in Fuke's 2D model.
4. For the ellipsoid workpiece, the long-axis direction has a more even thickness distribution than the transverse direction, indicating the need for the non-axial symmetric model.

Acknowledgment

Y.F. Li greatly appreciates the support from Tianjin Education Scientific Research Project (2018KJ204) and China Scholarship Council (CSC) Scholarship. This work is partially supported by the "Human Resources Program in Energy Technology (No.20194030202450)" of the Korea Institute of Energy Technology Evaluation and Planning (KETEP), granted financial resources from the Ministry of Trade, Industry & Energy (MOTIE), Republic of Korea.

References

1. Schiller, S., U. Heisig, and S. Panzer, *Electron Beam Technology*. 1982, New York: Wiley.
2. Fuke, I., V. Prabhu, and S. Baek, *Computational Model for Predicting Coating Thickness in Electron Beam Physical Vapor Deposition.* Journal of Manufacturing Processes, 2005. **7**(2): p. 140-152.
3. Guo, X., et al., *Novel Lanthanum Zirconate-based Thermal Barrier Coatings for Energy Applications*. 2020.
4. Singh, J. and D.E. Wolfe, *Review Nano and macro-structured component fabrication by electron beam-physical vapor deposition (EB-PVD).* Journal of Materials Science, 2005. **40**(1): p. 1-26.
5. Hass, D.D., P.A. Parrish, and H.N.G. Wadley, *Electron beam directed vapor deposition of thermal barrier coatings.* 1998. **16**(6): p. 3396-3401.
6. Zhang, D., *Thermal barrier coatings prepared by electron beam physical vapor deposition (EB–PVD)*, in *Thermal Barrier Coatings*, H. Xu and H. Guo, Editors. 2011, Woodhead Publishing. p. 3-24.
7. Mao, K., et al. *Coating Thickness Modeling and Prediction for Hot-dip Galvanized Steel Strip Based on GA-BP Neural Network.* in *2020 Chinese Control And Decision Conference (CCDC)*. 2020. Hefei, China.
8. Cho, S., et al., *Intelligent automation of electron beam physical vapour deposition.* Surface Engineering, 2005. **21**(1): p. 17-26.
9. Xie, X. and Y. Wang, *Research on Distribution Properties of Coating Film Thickness from Air Spraying Gun-Based on Numerical Simulation.* 2019. **9**(11): p. 721.
10. de Matos Loureiro da Silva Pereira, V.E., J.R. Nicholls, and R. Newton, *Modelling the EB-PVD thermal barrier coating process: Component clusters and shadow masks.* Surface and Coatings Technology, 2017. **311**: p. 307-313.
11. Li, Y., et al., *Finite element modeling of coating thickness using heat transfer method.* CIRP Journal of Manufacturing Science and Technology, 2021. **32**: p. 249-256.